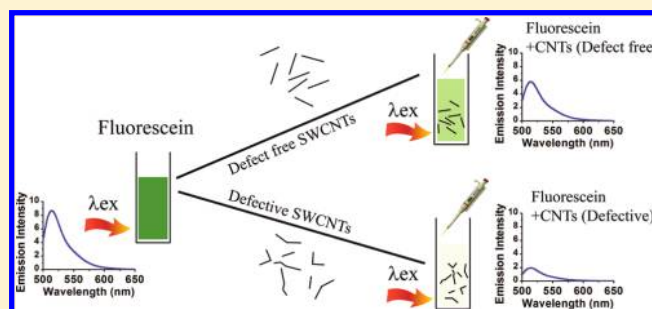


# Evidence for Defect-Enhanced Photoluminescence Quenching of Fluorescein by Carbon Nanotubes

Dilip K. Singh,<sup>†</sup> P. K. Giri,<sup>\*,†,‡</sup> and Parameswar K. Iyer<sup>\*,§</sup><sup>†</sup>Centre for Nanotechnology, <sup>‡</sup>Department of Physics, <sup>§</sup>Department of Chemistry, Indian Institute of Technology Guwahati, Guwahati-781039, India

**ABSTRACT:** We report on the definite role of surface defects in carbon nanotubes in the efficient photoluminescence (PL) quenching of fluorescein by single-walled (SWCNTs) and multi-walled carbon nanotubes (MWCNTs). Steady-state PL measurements show that SWCNTs are much more efficient quenchers than MWCNTs. The Stern–Volmer plot is found to follow a faster than exponential growth behavior for SWCNTs. Time resolved PL studies confirm a negligible contribution of dynamic quenching to the observed effect. Vacuum annealed SWCNTs containing fewer defects show very low quenching efficiency, though it exhibited high surface adsorption. A contribution of surface defects was further confirmed from study of quenching effects from a different set of SWCNT with high structural perfection, evidenced from Raman and thermogravimetric analysis. The mechanism of large quenching in SWCNTs is elucidated through systematic studies of absorption and emission spectroscopy.



## 1. INTRODUCTION

Fluorescence quenching is an important tool for studying biochemical systems and finds major applications in biosensing and imaging. In recent years, experiments have shown that single-walled carbon nanotubes (SWCNTs) act as an efficient photoluminescence (PL) quencher for a wide range of materials like fluorophores,<sup>1</sup> quantum dots,<sup>2</sup> porphyrin,<sup>3</sup> and polythiophene.<sup>4</sup> It has been suggested that SWCNTs statically quench the PL of the fluorophore by forming a stable ground state complex. On the basis of the quenching property, novel applications have recently been demonstrated including quantification of nanotube dispersion with chiral selection<sup>1</sup> and fluorescence imaging of nanotubes.<sup>5</sup> It has been reported that PL from SWCNTs are efficiently quenched by nitroaromatic functionalization.<sup>6</sup> Thus, the surface condition of SWCNTs seems to play an important role in the quenching process. A number of physical processes have been accounted for the quenching effect of carbon nanotubes (CNTs), such as, nonfluorescent complex formation with the fluorophores,<sup>7</sup> resonant energy transfer,<sup>8</sup> and electron transfer through  $\pi$ – $\pi$  interactions with compounds that possess a  $\pi$ -electron rich structure.<sup>1</sup> Previous studies have found chirality dependence for the quenching efficiency of SWCNTs.<sup>1</sup> However, no quantitative analysis has been attempted for the highly nonlinear Stern–Volmer plot observed for the reported quenching. While it is clear that the presence of multiple species of SWCNTs cannot account for such nonlinearity, a possible contribution of structural defects inherently present in as-grown and purified SWCNTs has not been considered in such analysis. Aashi et al. have demonstrated an ultrasensitive method for detection of DNA and antigen based on PL quenching by

CNTs.<sup>9</sup> Since efficient PL quenching by CNTs is highly desirable for applications like biomarkers and biosensors, it is imperative to understand the factors that control the quenching most. This would enable tenability of quenching efficiency of CNTs for various applications. Note that the absorption spectrum of typical SWCNTs spans over  $\sim$ 500–900 nm, significantly overlapping the PL emission spectra of various fluorophores. This may allow Fröster resonant energy transfer (FRET) to occur that would quench the PL of fluorophores.<sup>10</sup>

It is now widely accepted that defects in the carbon nanotube wall strongly influence the intrinsic properties of CNTs. Defect engineering of CNTs enables improved dispersion,<sup>11</sup> chemical functionalization,<sup>12</sup> sensing,<sup>13,14</sup> doping, and tuning of electronics,<sup>15</sup> as well as optical properties.<sup>16</sup> Furthermore, it has been proposed that defects in the nanotube walls and bundling of SWCNT can partially quench intrinsic PL of the nanotubes.<sup>17</sup> It has also been shown that defects in SWCNTs can disrupt the  $\pi$ – $\pi$  interaction between polythiophene and the nanotube's hybrid structure, which reduces the PL quenching efficiency as a result of reduced electron transfer. Thus, there are unanswered questions about the role of defects in the PL quenching of SWCNTs.

We have studied the role of structural defects on the PL quenching efficiency of SWCNTs and multi-walled carbon nanotubes (MWCNTs) on fluorescein, a widely used fluorophore. The influence of structural defects in the PL quenching

Received: August 2, 2011

Revised: October 30, 2011

Published: November 01, 2011

has been elucidated by comparing results of purified pristine SWCNTs containing surface defects and vacuum annealed SWCNTs containing fewer defects, as confirmed from Raman and thermogravimetric (TGA) studies.<sup>18</sup> Defect enhanced PL quenching efficiency has been further confirmed through systematic study with another SWCNT sample with higher structural perfection. The mechanism of quenching including the nature of interactions is elucidated through systematic studies of absorption and emission spectroscopy.

## 2. EXPERIMENTAL SECTION

SWCNTs (SWCNT-A) and MWCNTs used in this study are grown by chemical vapor deposition (CVD) and are commercially procured after standard purification. The SWCNTs have diameter <2 nm and a length of 5–15  $\mu\text{m}$ , while the MWCNTs have a diameter in the range 10–20 nm and a length in the range 5–15  $\mu\text{m}$ .<sup>18</sup> The as-purified SWCNTs contain a substantial amount of structural defects as evidenced from Raman and TGA studies, reported earlier.<sup>18</sup> For comparison, another set of SWCNT samples with higher structural perfection (grown by the electric arc evaporation method in Fraunhofer Institute for Material and Beam Technology, Germany) was used. This sample is termed as SWCNT-B. TGA studies were carried out using a commercial TGA apparatus (Metler-Teledo TGA 1100) under a 40 sccm flow of air, and the heating rate was kept at 5  $^{\circ}\text{C}/\text{min}$ . Raman measurements were performed using a 632.8 nm He–Ne laser excitation and a commercial high resolution micro-Raman spectrometer (Jovin Horiba, LabRam HR800). Some of the SWCNT-A samples are high-vacuum ( $1 \times 10^{-6}$  mbar) annealed at 700  $^{\circ}\text{C}$  for 2 h to remove structural defects<sup>18</sup> and studied. These annealed samples are termed as SWCNT-VA. A standard fluorophore solution of 2  $\mu\text{M}$  concentration was prepared to avoid high optical density and turbidity. For experiments, to prepare micromolar solutions of fluorescein we added a very small amount of fluorophores to a 0.1 M NaOH solution, and its absorbance was adjusted to ensure the concentration was equal to 2  $\mu\text{M}$ . Use of micromolar concentration was essential to avoid the self-quenching of fluorescence. Such a low concentration ensures the absence of two adjacent fluorophore molecules. Self-quenching is not possible due to the absence of molecular aggregation. A fluorescein solution was prepared in 0.1 M NaOH. The concentration of fluorescein was estimated using the extinction coefficient ( $\alpha = 68908 \text{ cm}^{-1}/\text{m}$ ) at absorption wavelength ( $\lambda_{\text{abs}} = 496 \text{ nm}$ ) from the Beer–Lambert law. For adsorption analysis, the Beer–Lambert law was used to estimate the concentration of fluorophore before and after the addition of CNTs. An adsorbed amount of fluorophore was estimated after subtracting the value of the concentration of fluorophore before and after the addition of CNTs in each step. Weight of the fluorophore adsorbed [A] was calculated by dividing the number of micromoles to the molecular weight; 332.31 g for fluorescein. Steady-state PL measurements were performed using a commercial fluorimeter (Thermo Electron, FA-357). In each step, 40  $\mu\text{L}$  of the standard fluorophore solution was taken out, and 40  $\mu\text{L}$  of the nanotube solution was added continuously to 3 mL of the standard fluorophore solution taken in a 10 mm quartz cuvette so that the concentration of fluorophore remains constant. Time-resolved photoluminescence (TRPL) measurements were performed using Life Spec II Edinburgh Instruments with a time resolution of 50 ps. For TRPL measurements, fluorescein was excited with a 475 nm laser, and emission was monitored at 513 nm.

## 3. RESULTS AND DISCUSSION

Fluorescein shows a PL emission peak at 513 nm when excited with 496 nm. Figure 1a shows a decrease in the PL intensity of fluorescein with an increasing concentration of SWCNT-A. Figure 1b shows the change in the PL intensity ratio before and after the addition of SWCNT-A, known as a Stern–Volmer plot. This plot shows a quenching efficiency of  $\sim 98.1\%$  for the pristine SWCNT-A. Figure 1c shows that the PL quenching efficiency of MWCNTs is very low compared to that of SWCNT-A. Figure 1d shows the Stern–Volmer plot for MWCNTs along with the SWCNT-A and SWCNT-VA containing fewer defects. It is very interesting to note that the quenching efficiency of SWCNT-VA is dramatically low (65.6%) as compared to that of unannealed SWCNT-A (98.1%), and it is the lowest among all samples. The nonlinear nature of the Stern–Volmer plot in Figure 1b for SWCNT-A indicates the presence of a combined effect of static and dynamic quenching.<sup>19</sup> When a fluorophore is quenched by collisions as well as by complex formation, it is represented by a nonlinear equation in concentration:  $F_0/F = 1 + (K_D + K_S)[Q] + K_D K_S [Q]^2$ , where  $[Q]$  is the concentration of the nanotube, and  $K_S$  and  $K_D$  are static and dynamic Stern–Volmer constants, respectively. For the data plotted in Figure 1b,  $(F_0/F - 1)/[Q]$  versus  $[Q]$  was found to be highly nonlinear, similar to that found in ref 1. The nonlinear nature of the Stern–Volmer plot indicates the involvement of other factors apart from static quenching like dynamic quenching, possibility of FRET leading to higher quenching efficiency observed, higher probability of quenching represented by sphere of action model, or rearrangement of molecules. A minor contribution of dynamic quenching has been found as estimated through TRPL studies presented later. Interestingly, the present data follows a compressed-exponential (faster than exponential growth) behavior given by:  $F_0/F = \exp(b[Q])^\alpha$ , with  $b = 0.0149$  and  $\alpha = 1.307$ . This is in contrast to that reported for Rhodamine B.<sup>1</sup> It may be noted that our quenching studies on Rhodamine 6G and Quinine sulfate show qualitatively similar behavior. However, in the case of Rhodamine 6G, the efficiency of quenching is relatively higher (99.87%). Note that when the extent of quenching is large, the usual Stern–Volmer equation is not obeyed. In the literature, a large quenching behavior has been explained in terms of the sphere of action model when the fluorophore and quencher are closely spaced.<sup>19</sup> The sphere of action is expressed by the modified form of the Stern–Volmer equation given by  $F_0/F = (1 + K_D[Q]) \exp([Q]VN/1000)$ , where  $V$  is the volume of the sphere. This equation modifies to purely exponential growth when the contribution of dynamic quenching is negligible, i.e.,  $K_D \approx 0$ . As discussed below, the time-resolved PL studies indeed show that dynamic contribution to the observed quenching is extremely small as compared to the static contribution. However, for the defective SWCNTs, these results follow a compressed-exponential growth behavior due to the long cylindrical structure of the quenchers (in this case CNTs), in contrast to the small volume of the spherical shape of the quenchers as assumed in the sphere of action model. We believe that due to the presence of defects on the CNT surface, the quenching efficiency is extremely high that follows a faster-than exponential behavior with  $\alpha = 1.307$ , as compared to the modified Stern–Volmer equation with  $\alpha = 1$ . In the case of SWCNT-VA, it was found to follow  $\alpha = 1.032$  (i.e., nearly 1), while MWCNTs follows the modified Stern–Volmer equation perfectly with  $\alpha = 1$ . Though a compressed-exponential growth is uncommon in physical systems,

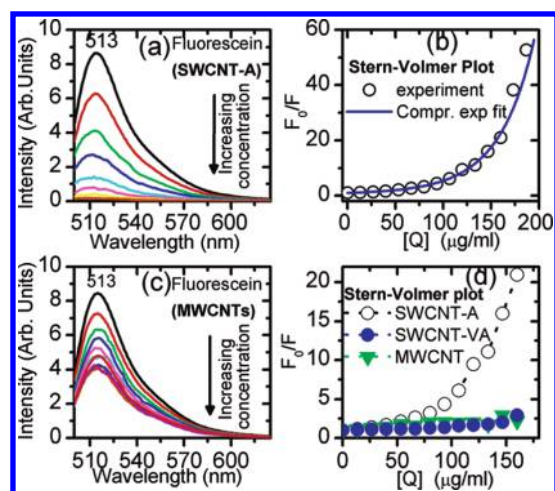


**Figure 1.** (a) Steady-state PL spectra showing the quenching effect on fluorescein with different concentrations of SWCNTs. (b) Stern–Volmer plot with a compressed-exponential fit. See text for more details. (c) Quenching effect due to MWCNTs. (d) Comparison of quenching efficiency for SWCNTs, SWCNT-VA, and MWCNTs.

Baouchaud and Pitard suggested recently a specific model for the compressed-exponential that can occur from local rearrangement of molecules or microcollapse of particles.<sup>20</sup> Such rearrangement of molecules is quite plausible in the case of adsorption of fluorophores on CNTs with highly reactive sites due to the presence of defects.

In order to assess the role of structural defects, dangling bonds, and impurities in the quenching, we systematically studied the quenching efficiency for graphite powder, SWCNTs functionalized with a COOH group, activated charcoal, and MWCNTs containing extremely low catalyst content. The nature of defects are different in SWCNTs and MWCNTs. SWCNTs contains defects like pentagon–heptagon rings, Stone–Wales defects, and vacancies that can tailor its band gap and optical properties, leading to observed enhanced PL quenching effect. However, MWCNTs contains defects like intershell linkages and staking faults in the multilayer structure. Further, SWCNTs show a self-healing capacity, while MWCNTs do not show such behavior. A difference in the nature of defects between SWCNTs and MWCNTs is due to their different growth conditions and amount of lattice strains involved. Smaller diameter tubes (usually SWCNTs) have higher lattice strain, while MWCNTs (larger in diameter) have lower lattice strain. Note that graphite powder shows a linear Stern–Volmer plot, while activated charcoal shows a nonlinear plot, both with very low quenching efficiency. A very low amount of amorphous carbon in SWCNT-A along with other phases of carbon (<5 wt % as estimated from TGA) that have only ~62.5% quenching efficiency cannot account for the highly nonlinear Stern–Volmer plot observed for SWCNT-A. Therefore, defects and dangling bonds on the surface of the SWCNTs are likely to contribute to the observed high quenching efficiency.

Figure 2 shows TRPL analysis to elucidate the contribution of dynamic quenching. Figure 2a shows typical PL decay dynamics for fluorescein with a single exponential fit. Before the addition of SWCNT-A, it shows a decay time constant ( $\tau_0$ ) of 4.05 ns. Figure 2b shows the monotonic decrease in the PL lifetime of fluorescein upon the addition of SWCNT-A. This is due to the diffusion of CNTs to the fluorophore during the lifetime of the

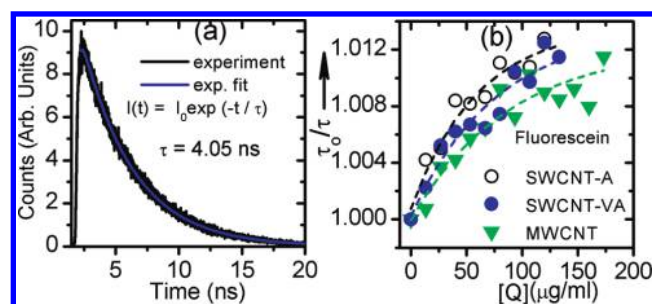


**Figure 2.** (a) Time-resolved PL spectra of fluorescein. (b) Change in PL lifetime ratio ( $\tau_0/\tau$ ) before and after adding SWCNTs, SWCNTs-VA, and MWCNTs as quenchers. Dashed line in each case represents a guide to the eye.

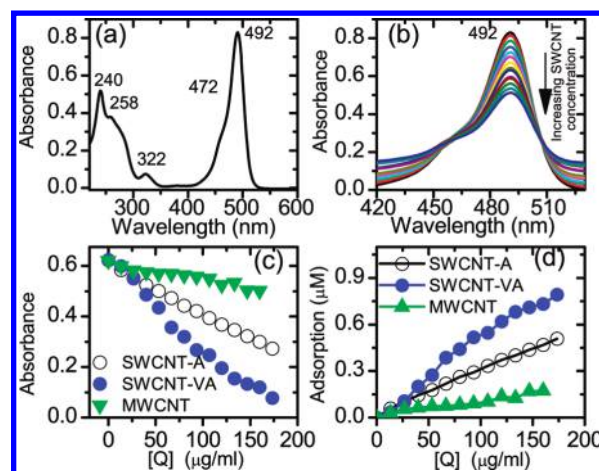


**Figure 3.** (a) Typical absorption spectra of fluorescein with a major peak at 492 nm. (b) Change in the absorbance of fluorescein with an increasing concentration ( $[Q]$ ) of SWCNT-A. (c) Comparison of absorbance for SWCNT-A, SWCNT-VA, and MWCNT as a function of  $[Q]$ . (d) Comparison of adsorption isotherms for SWCNT-A, SWCNT-VA, and MWCNT.

excited state. Note that for a perfect dynamic quenching,  $F_0/F$  is equal to  $\tau_0/\tau$ .<sup>19</sup> However, experimental data shows a very minor change in  $\tau_0/\tau$  as compared to the large change in  $F_0/F$ . This implies that the contribution of dynamic quenching is very insignificant to the observed effect. Therefore, the coefficient of dynamic quenching  $K_D$  is considered very small compared to the coefficient of static quenching  $K_S$ . Thus, the static quenching is primarily responsible for the observed nonlinear quenching behavior, and this is in agreement with reported results on a different fluorophore.<sup>1</sup> Note that from TRPL studies,  $K_D$  is found to be negligible compared to  $K_S$  in all the three samples, i.e., SWCNT, SWCNT-VA, and MWCNT.

Static quenching can arise due to the formation of a non-fluorescent complex between the fluorophore and the quencher. When this complex absorbs light, it immediately returns to the ground state without emission of a photon. This is expected to show a shift in the absorption spectra. However, our results do not show any measurable shift in absorption peak wavelength, as shown in Figure 3b, eliminating the possibility of nonfluorescent complex formation. Figure 3b shows a systematic decrease in absorption intensity after the addition of SWCNT-A at different concentrations. An electrostatic interaction may also lead to a

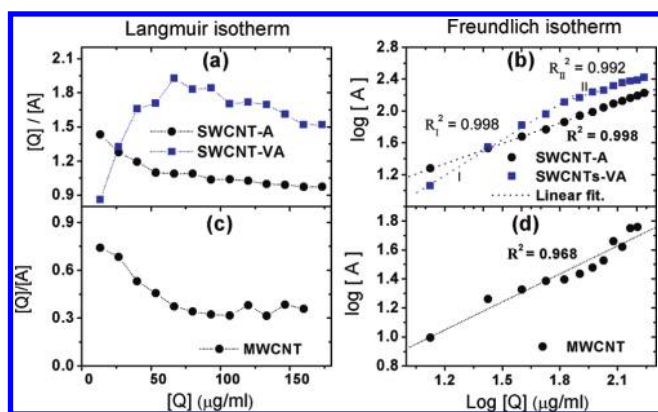


**Figure 4.** Langmuir (left side) and Freundlich isotherm (right side) models for adsorbed fluorophores on the CNT surface. Adsorption of fluorescein on SWCNT-A and SWCNT-VA surface is shown by the (a) Langmuir isotherm and (b) Freundlich isotherm. Linear fit to the experimental data points are shown by a dotted line. The Freundlich isotherm model best fits to the experimental data points indicating a multilayer adsorption. Panels c and d show Langmuir and Freundlich isotherm for the adsorption of fluorescein on MWCNT.

decrease in the PL intensity through the adsorption of fluorophores on the CNT walls, inside the tubes, and trapping in bundles. Figure 3c shows a comparison of change in the absorbance of fluorescein as a function of added concentration of SWCNT-A, SWCNT-VA, and MWCNT.

The length of CNTs may have influence on the results since longer length tubes would have more area for adsorption or interaction with fluorophores. However, we have used CNTs grown in the same batch, and they are expected to have similar lengths with a statistical distribution. Furthermore, during our experiments we have dealt with the weight of the CNTs to represent  $[Q]$ . So, the effect of the length is not explicitly reflected in the results. Since the CNT solution was initially prepared with a concentration of 1 mg/mL fluorophore solution, the addition of 40  $\mu\text{L}$  represents the addition of 40  $\mu\text{g}$  of CNTs to 3 mL of the fluorophore solution. Figure 3d shows a quantitative comparison of amounts of fluorescein adsorbed by SWCNT-A, SWCNT-VA, and MWCNT. The amount of fluorescein adsorbed by SWCNT-VA is much larger than the pristine SWCNT-A (with defects) and MWCNT. It is clear that MWCNT shows a minimum adsorption of fluorescein. We have found<sup>18</sup> that the CVD grown pristine SWCNT-A contains a large amount of defects that can be substantially removed by vacuum annealing at 700  $^{\circ}\text{C}$ , as shown later. These annealed samples have higher thermal stability and a higher G'-band to D-band intensity ratio in the Raman spectra.<sup>18</sup> Pristine SWCNT-A (with defects) show lesser adsorption but have stronger quenching efficiency. Thus, surface adsorption cannot fully account for the extent of quenching observed. We believe that highly nonlinear quenching behavior observed here is partly contributed by FRET. FRET is based on the concept of fluorophore as an oscillating dipole, which can exchange energy with another dipole with a similar resonance frequency. Structural defects in the CNTs can increase the dipole moment and interact more efficiently with the fluorophore in the close vicinity, as expected in the sphere of action model. When the fluorophore and the quencher are very close, there exists a high probability that quenching will occur before these molecules diffuse apart. As the quencher concentration increases, the probability that a quencher is within the first

solvent shell of the fluorophore at the moment of excitation increases. CNTs with sidewall defects can have enhanced  $\pi-\pi$  interaction with the fluorophore that would enable close by spacing of the fluorescein and the CNT molecules. Because of the large size of the quencher, a large number of fluorophore molecules interact simultaneously with the defect sites of the SWCNTs and give rise to strong quenching behavior.

Since we did not observe any shift in the emission spectra (as well as absorption spectra) of fluorescein with the addition of CNTs, this indicates that the interaction between fluorescein and SWCNT is  $\pi-\pi$ . In order to explore the nature of the interaction between SWCNTs and fluorescein in more detail, the adsorption of fluorescein was analyzed using Langmuir and Freundlich isotherms. The Langmuir isotherm model represents monolayer adsorption of molecules on the surface, whereas the Freundlich isotherm represents multilayer adsorption of molecules on the surface. The Langmuir isotherm is expressed as

$$[A] = \frac{Q_m b [Q]}{1 + b [Q]} \text{ or } \frac{[Q]}{[A]} = \frac{1}{Q_m b} + \frac{1}{Q_m} [Q] \text{ (Linear in } [Q]) \quad (1)$$

and the Freundlich isotherm is expressed as

$$[A] = K_f [Q]^{1/n} \text{ or } \log[A] = \log K_f + \frac{1}{n} \log[Q] \text{ (Linear form)} \quad (2)$$

where,  $[A]$  is the amount of fluorophore adsorbed by  $[Q]$  weight of CNTs.  $Q_m$  represents the maximum adsorption capacity,  $K_f$  is the Freundlich affinity coefficient, and  $n$  represents the Freundlich exponent factor. From Figure 4, linear behavior is expected if it follows a particular isotherm, either the Langmuir isotherm or the Freundlich isotherm. Figure 4a,b shows Langmuir and Freundlich isotherms, respectively, for fluorescein adsorbed on SWCNT-A and SWCNT-VA. The behavior of the Langmuir isotherm in this case is far from being linear, whereas the Freundlich isotherm shows an excellent fit to the data points giving  $R^2 = 0.997$ , where  $R^2$  being closer to 1.0 is a measure of the quality of fit. The value of the slope and intercept obtained from the linear fit to eq 2, i.e.,  $\log[A]$  vs  $\log[Q]$ , give values of the inverse of the Freundlich exponent factor ( $n$ ) and log of the Freundlich affinity coefficient  $K_f$ . The value of the Freundlich exponent factor ( $n$ ) comes out to be 1.174 for SWCNT-A; that indicates a contribution of adsorption, as it is within a range of 1–10.<sup>21</sup> In the case of SWCNT-VA, adsorption behavior can be divided into two segments, one for lower concentration and another for higher concentration of nanotubes due to the difference in interaction for adsorption in the two concentration ranges, both giving excellent  $R_1^2 = 0.988$  and  $R_{II}^2 = 0.992$  values. For SWCNT-VA, the value of  $n$  was found to be 0.66 at lower concentration and 1.35 at higher concentration regions. High CNT concentration may influence the physical characteristics of the solid–liquid suspensions, such as by increasing the viscosity and inhibiting the diffusion. Figure 4c shows the Langmuir isotherm and Figure 4d the Freundlich isotherm for MWCNT-A. It is interesting to note that the behavior of MWCNT-A is similar to the annealed sample SWCNT-VA in the Langmuir isotherm, and it is not linear in behavior. This indicates that the Langmuir model poorly represents the physical process of adsorption in this case. However, linear fitting with the Freundlich model shows a  $R^2 = 0.968$ ,

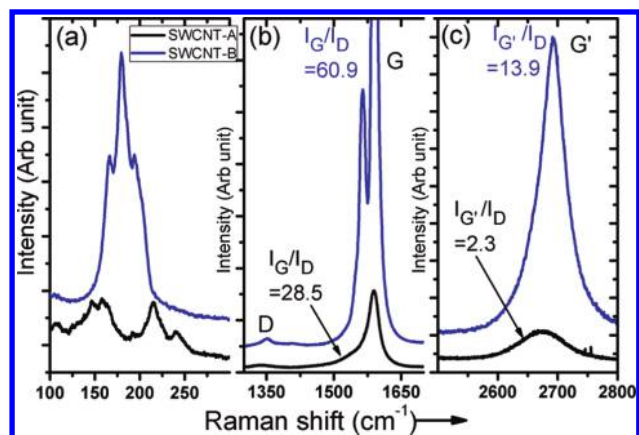


**Figure 5.** Comparison of Raman spectra of SWCNT-A and SWCNT-B: (a) RBM modes, (b) D and G bands, and (c)  $G'$  mode. The ratio of intensities of the G to D bands and  $G'$  band to D band are shown in the figure. As compared to SWCNT-A, SWCNT-B shows much higher  $I_G/I_D$  and  $I_{G'}/I_D$  ratios indicating higher structural perfection/fewer defects in SWCNT-B.

indicating that the quenching process does not follow the Freundlich model properly. In the case of adsorption of fluorescein on MWCNTs, the value of  $n$  was found to be 1.548. Thus, from this study it is clear that adsorption of fluorophores on the CNTs take the form of multilayer adsorption of molecules. A slight deviation observed from the Freundlich model represents fluctuations arising from the probabilistic nature of the adsorption sites leading to the slight nonlinearity. Although there has been an attempt to model this with nonlinear models, like the Brunauer–Emmett–Teller model (BET) and Polanyi–Manes model (PMM),<sup>22</sup> but within the experimental error and taking into consideration the various factors related to CNTs such as structure, purity, dispersibility problem, etc., the Freundlich model is found to best represent the physical process of adsorption of fluorophores on the nanotube surface. A large value of the Freundlich exponent factor ( $n$ ) for SWCNT-A shows higher adsorption on SWCNT than the MWCNT. In agreement to our results, other studies on organic chemical adsorption on CNTs through adsorption isotherms modeling have shown that SWCNTs are heterogeneous adsorbents, and the Freundlich equation describes well the interaction between organic molecules and SWNTs.<sup>23</sup>

Furthermore, to confirm the definite role of defects in the photoluminescence quenching efficiency of SWCNTs, we performed experiments with another set of SWCNTs (sample SWCNT-B) with high structural perfection, as confirmed from Raman spectroscopy and thermogravimetric measurements. Figure 5 shows the Raman spectra for SWCNT-A and SWCNT-B recorded under similar experimental conditions. Both the samples show (Figure 5a) clear radial breathing modes (RBMs) confirming the single-walled nature of the nanotubes. The characteristic D and G modes are shown in Figure 5b, while the second order  $G'$ -mode is shown in Figure 5c. Note that both the samples show a reasonably high ratio of intensity of the G band to D band ( $I_G/I_D$ ), confirming the good quality of the samples. However, SWCNT-B shows a much higher  $I_G/I_D$  ratio and the higher  $G'$  band to D bands ratio ( $I_{G'}/I_D$ ), as indicated in respective plots. The  $I_{G'}/I_D$  ratio is taken as a standard of measure of structural perfectness of CNTs.<sup>24</sup> SWCNT-A shows a  $I_{G'}/I_D$  ratio of 2.3, while SWCNT-B shows a  $I_{G'}/I_D$  ratio of

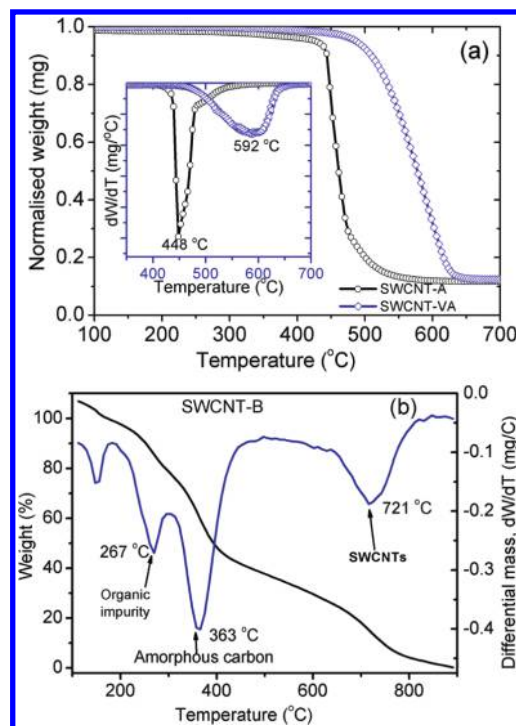


**Figure 6.** (a) Comparison of TGA spectra for SWCNT-A and SWCNT-VA. Inset shows the corresponding DTA spectra showing an oxidation temperature of 448 and 592 °C for SWCNT-A and SWCNT-VA, respectively. (b) TGA/DTA spectra of SWCNTs-B showing a comparatively higher oxidation temperature of 721 °C for SWCNTs. It also shows the presence of carbonaceous impurities ( $T_{ox} = 363$  °C) and organic impurities ( $T_{ox} = 151$  and 267 °C) as indicated in the figure.

13.9. Such a higher value of  $I_{G'}/I_D$  ratio clearly indicates that SWCNT-B contains fewer defects in comparison to SWCNT-A.

The higher structural perfection of the SWCNT-B is further confirmed from TGA analysis. Figure 6a shows the comparison of TGA (solid curve) data for SWCNT-A and SWCNT-VA, and the inset shows the corresponding DTA spectra. DTA spectra of SWCNT-A show a major oxidation peak at 448 °C, while that of SWCNT-VA shows a higher oxidation temperature of 592 °C. The oxidation temperature of vacuum annealed SWCNT samples is considerably increased from that of the pristine SWCNT-A due to the removal of structural defects during annealing. Figure 6b shows the TGA and DTA spectra of SWCNT-B. The DTA curve of SWCNTs-B shows peaks at 267, 363, and 721 °C, corresponding to the burning/oxidation of organic impurities, amorphous carbon, and SWCNTs, respectively. Since the starting SWCNT-B sample was taken in paste form (made with deionized water), low temperature peaks corresponding to the moisture and organic impurities are observed. However, SWCNT-B showing an oxidation temperature of 721 °C clearly shows that these are of higher structural perfection than the SWCNT-A with a lower oxidation temperature of 448 °C. It is well-known that defective CNTs show a lower oxidation temperature.<sup>25</sup> Thus, it is clear that SWCNTs-B contains fewer defects than the SWCNTs-A, and this is fully consistent with the results of Raman analysis.

Figure 7a shows the decrease in PL intensity of fluorescein with an increasing concentration of SWCNT-B, a sample containing fewer defects. A corresponding Stern–Volmer plot is shown in Figure 7b, and it is linear in nature. Very low quenching efficiency of SWCNT-B is observed as indicated by a lower value of  $F_0/F$  in

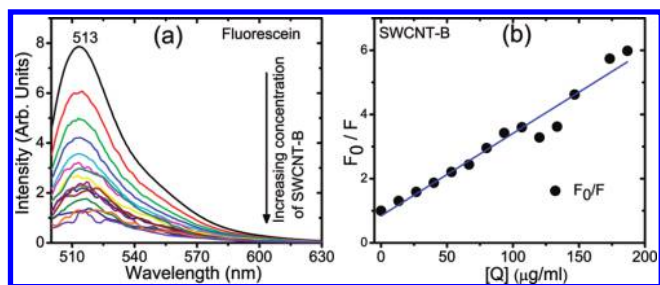


**Figure 7.** (a) Photoluminescence quenching of fluorescein by the less defective sample (SWCNT-B). (b) Stern–Volmer plot showing the linear nature and comparative lower PL quenching efficiency for SWCNT-B.

comparison to those of SWCNT-A and SWCNT-VA. This confirms the important role of defects toward the high photoluminescence quenching effect observed in SWCNT-A. The linear nature of the Stern–Volmer plot in SWCNT-B may arise due to the negligibly small contribution of dynamic quenching owing to a higher tendency of bundling that leads to a decrease in diffusion of SWCNT-B in the fluorescein solution. There exists a possibility that during vacuum annealing a portion of SWCNTs may convert to MWCNTs that leads to a lower quenching efficiency of SWCNT-VA. Such a possibility is ruled out by studying the quenching effect with SWCNT-B that contains fewer structural defects. The comparatively lower quenching efficiency ( $\sim 83.3\%$ ) of SWCNT-B as compared to SWCNT-A (98.1%) clearly demonstrates that structural defects in SWCNTs enhance the quenching effect dramatically.

#### 4. CONCLUSIONS

We have demonstrated that structural defects in SWCNTs strongly influence the PL quenching efficiency for standard fluorophores. SWCNTs with surface defects were found to be highly efficient (98.1%) quenchers as compared to the MWCNTs and SWCNTs with high structural perfection. For defective SWCNTs, a Stern–Volmer plot was found to follow a compressed-exponential behavior due to the large size of the quenchers as compared to the size of the fluorophore. Through TRPL studies, we have shown that static quenching is primarily responsible for the observed quenching. Defective SWCNTs were found to adsorb less as compared to the near-perfect SWCNTs. The nature of interaction between the fluorophore and CNT molecule is further explored by the Freundlich isotherm model that confirms multilayer adsorption. We provided evidence that besides the surface adsorption, FRET is most likely to be responsible for the high efficiency of quenching. These results demonstrate that control and manipulation of defects in CNTs would enable enhanced quenching efficiency for various biological applications.

#### AUTHOR INFORMATION

##### Corresponding Author

\*(P.K.G.) Phone: +91-361-258-2703. Fax: +91-361-258-2749. Email: giri@iitg.ernet.in. (P.K.I.) Phone: +91-361-258-2314. Fax: +91-361-258-2349. E-mail: pki@iitg.ernet.in.

#### REFERENCES

(1) Ahmad, A.; Kurkina, T.; Kern, K.; Balasubramanian, K. *ChemPhysChem* **2009**, *10*, 2251–2255.

- (2) Pan, B. F.; Cui, D. X.; Ozkan, C. S.; Ozkan, M.; Xu, P.; Huang, T.; Liu, F. T.; Chen, H.; Li, Q.; He, R.; Gao, F. *J. Phys. Chem. C* **2008**, *112*, 939–944.
- (3) Casery, J. P.; Bachilo, S. M.; Weisman, R. B. *J. Mater. Chem.* **2008**, *18*, 1510–1516.
- (4) Geng, J.; Kong, B.; Yang, S. B.; Youn, S. C.; Park, S.; Joo, T.; Jung, H. *Adv. Funct. Mater.* **2008**, *18*, 2659–2665.
- (5) Prakash, R.; Washburn, S.; Superfine, R.; Cheney, R. E.; Falvo, M. R. *Appl. Phys. Lett.* **2003**, *83*, 1219–1221.
- (6) Kose, M. E.; Harruff, B. A.; Lin, Y.; Veca, L. M.; Lu, F.; Sun, Y. *J. Phys. Chem. B* **2006**, *110*, 14032–14034.
- (7) Martin, R. B.; Qu, L.; Lin, Y.; Harruff, B. A.; Bunker, C. E.; Gord, J. R.; Allard, L. F.; Sun, Y. *J. Phys. Chem. B* **2004**, *108*, 11447–11453.
- (8) Yanagi, K.; Iakubovskii, K.; Matsui, H.; Matsuzaki, H.; Okamoto, H.; Miyata, Y.; Maniwa, Y.; Kazaoui, S.; Minami, N.; Kataura, H. *J. Am. Chem. Soc.* **2007**, *129*, 4992–4997.
- (9) Cui, D.; Pan, B.; Zhang, H.; Gao, F.; Wu, R.; Wang, J.; He, R.; Asahi, T. *Anal. Chem.* **2008**, *80*, 7996–8001.
- (10) Biju, V.; Itoh, T.; Baba, Y.; Ishikawa, M. *J. Phys. Chem. B* **2006**, *110*, 26068–26074.
- (11) Kim, J. H.; Kataoka, M.; Shimamoto, D.; Muramatsu, H.; Jung, Y. C.; Tojo, T.; Hayashi, T.; Kim, Y. A.; Endo, M.; Terrones, M.; Dresselhaus, M. S. *ChemPhysChem* **2009**, *10*, 2414–2417.
- (12) Kim, S. J.; Park, Y. J.; Ra, E. J.; Kim, K. K.; An, K. H.; Lee, Y. H. *Appl. Phys. Lett.* **2007**, *90*, 023114.
- (13) Feng, X.; Irle, S.; Witek, H.; Morokuma, K.; Vidic, R.; Borguet, E. *J. Am. Chem. Soc.* **2005**, *127*, 10533–10538.
- (14) Horváth, Z. E.; Koós, A. A.; Kertész, K.; Molnár, G.; Vértesy, G.; Bein, M. C.; Frigyes, T.; Mészáros, Z.; Gyulai, J.; Biró, L. P. *Appl. Phys. A: Mater. Sci. Process.* **2008**, *93*, 495–504.
- (15) Agrawal, S.; Raghuvver, M. S.; Li, H.; Ramanath, G. *Appl. Phys. Lett.* **2007**, *90*, 193104.
- (16) Wei, G. *Appl. Phys. Lett.* **2006**, *89*, 143111.
- (17) Carlson, L. J.; Maccagnano, S. E.; Zheng, M.; Silcox, J.; Krauss, T. D. *Nano Lett.* **2007**, *7*, 3698–3703.
- (18) Singh, D. K.; Iyer, P. K.; Giri, P. K. *J. Appl. Phys.* **2010**, *108*, 084313.
- (19) Lakowicz, J. R. *Principles of Fluorescence Spectroscopy*; Kluwer Academic Publishers: New York, 1999; Chapter 8.
- (20) Bouchaud, J. P.; Pitard, E. R. *Europhys. Lett.* **2001**, *6*, 231–236.
- (21) Hall, K. R.; Eagleton, L. C.; Acivos, A.; Vermeulen, T. *Ind. Eng. Chem. Fundam.* **1966**, *5*, 212–223.
- (22) Yang, K.; Zhu, L.; Xing, B. *Environ. Sci. Technol.* **2006**, *40*, 1855–1861.
- (23) Agnihotri, S.; Rood, M. J.; Rostam-Abadi, M. *Carbon* **2005**, *43*, 2379–2388.
- (24) Dileo, R. A.; Landi, B. J.; Raffaele, R. P. *J. Appl. Phys.* **2007**, *101*, 064307.
- (25) Bom, D.; Andrews, R.; Jacques, D.; Anthony, J.; Chen, B.; Meier, M. S.; Selegue, J. P. *Nano Lett.* **2002**, *2*, 615–619.